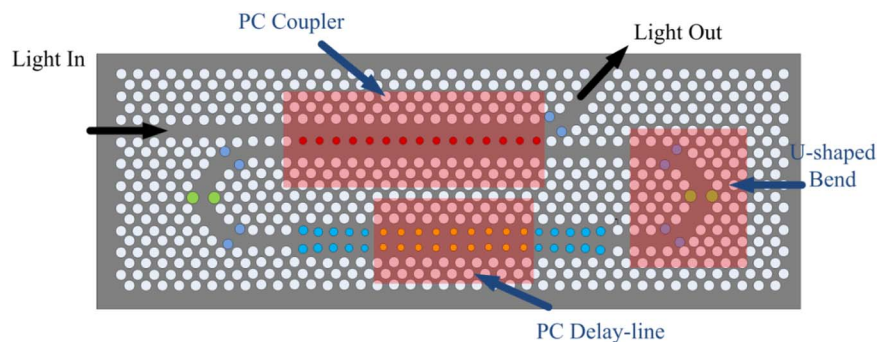


# Integration of Photonic Crystal Splitter and Slow Light Waveguide for a Microwave Photonic Filter

Volume 5, Number 4, August 2013

Guansheng Shen  
Huiping Tian  
Daquan Yang  
Yuefeng Ji



DOI: 10.1109/JPHOT.2013.2272777  
1943-0655/\$31.00 ©2013 IEEE

# Integration of Photonic Crystal Splitter and Slow Light Waveguide for a Microwave Photonic Filter

Guansheng Shen, Huiping Tian, Daquan Yang, and Yuefeng Ji

State Key Laboratory of Information Photonics and Optical Communications, School of Information and Telecommunication Engineering, Beijing University of Posts and Telecommunications, Beijing 100876, China

DOI: 10.1109/JPHOT.2013.2272777  
1943-0655/\$31.00 ©2013 IEEE

Manuscript received May 3, 2013; revised June 29, 2013; accepted July 1, 2013. Date of current version July 19, 2013. This work was supported in part by the National 973 Program under Grant 2012CB315705, by the National 863 Program under Grants 2011AA010305 and 2011AA010306, and by the Fund of the State Key Laboratory of Information Photonics and Optical Communications (Beijing University of Posts and Telecommunications), P. R. China. Corresponding authors: H. Tian and Y. Ji (e-mail: hptian@bupt.edu.cn; jyf@bupt.edu.cn).

**Abstract:** We theoretically investigate an ultracompact integration of a photonic crystal (PC) splitter and a slow-light waveguide for a microwave photonic filter. We realize the filter characteristics with a free spectrum range of 130 GHz and a notch depth of 10 dB, and the whole length is only 24.8  $\mu\text{m}$  with the use of a slow-light PC waveguide as a delay line. The splitter is fabricated with the delay line using a U-shaped waveguide. In addition, the coupling efficiency between slow-light waveguide and U-shaped waveguide has been increased from 10% to 62% with an optimized linear taper structure. The proposed microwave photonic filter can be applied in the 60-GHz Radio-over-Fiber (RoF) system.

**Index Terms:** Photonic crystals, optical interconnects, waveguide devices.

## 1. Introduction

With the growth in optical network technologies and wireless business requirements [1], Radio over Fiber system has been an increasing research since its centrally managed architecture, high broadband and low power consumption [2], [3]. The 60-GHz band is an unlicensed band of 9 GHz, which means 60-GHz RoF system can offer a huge free broadband application without physical interconnection [4]. Although standard-reach ( $\sim 20\text{km}$ ) ROF access network received more attention, there is little attention focused on long-reach ( $> 100\text{ km}$ ) ROF system. One of the possible reasons is that the long fiber can cause severe chromatic dispersion which adds different delays for sidebands and carrier [4]. For example, the Double Side Band (DSB) modulation could cause power fluctuation problem, while the Optical Carrier Suppression (OCS) modulation can also cause severe time-shifting of the data due to the chromatic dispersion by the two tones [5]–[7]. For these reasons, the Single Side Band (SSB) is a popular modulation for long distance RoF system.

To separate the carrier and needless side band, microwave photonic filter (MPF) is a key device for SSB RoF transmission. There are numerous different MPFs developed in the past few years, including silicon micro-ring resonator based MPFs [8], Mach–Zehnder Interferometer based MPFs [9], fiber ring resonator MPFs [10] and so on. During these methods, the optical ring resonator based on fiber loop should be the simplest way for Infinite Impulse Response (IIR) MPFs while Free Spectrum Range (FSR) is usually less than 1 GHz. But the RoF system needs a larger FSR of

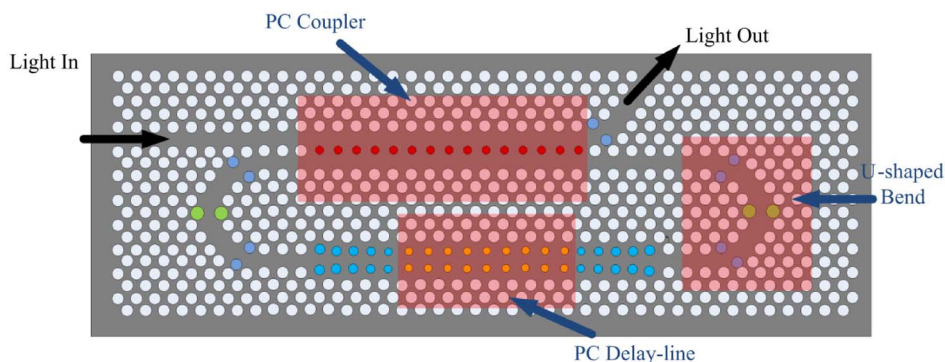


Fig. 1. Schematic of the photonic crystal MPF.

10 GHz level, and the delivery of millimeter-wave signals has a high propagation loss. So micro and pico-cellular architectures are applied in the RoF system. Therefore, the high integration density is necessary for base station (BS) and MPF based on fiber ring would increase the size of MPFs.

According to the formula  $FSR = C/n_g L$  [10], where  $C$  is the light speed in vacuum, and  $n_g$  and  $L$ , respectively, are the group index and length of delay-line for MPF, we can reduce the length of device by directly increasing the group index of delay line. For this reason, the slow light photonic crystal waveguide is a good choice since its high group index and low power consumption. It should be noted that the formula is different with silicon micro-ring resonator  $FSR = \lambda^2/n_g(2\pi R)$ , because photonic crystal has a good localization property and we need not consider the drop light power caused by resonator.

Photonic crystal (PC) is a material in which the refractive index is periodically changed. Photonic crystal structures have achieved a lot of attention since they allow for the integration of various active and passive devices [11]–[14]. Two-dimension simulation can be used to study the fundamental principles of PC structures in a simple way. And the design could be realized directly in three-dimensions using silicon on insulator (SOI) slab, whose weak vertical confinement allows it to reproduce results from two dimensional structures slab [15]–[21].

In this paper, we demonstrate an ultra-compact integration of a PC splitter and a slow light waveguide for microwave photonic filter in one SOI slab. We realize the filter characteristics with a free spectrum range of 130 GHz, a notch depth of 10 dB, and the whole length is only  $24.8 \mu\text{m}$  with the use of slow light PC waveguide as a delay line. For this design, the group index of PC slow light waveguide is above 110 calculated by two-dimensional simulation. And a U-shaped waveguide is used to combine the PC splitter and PC slow light waveguide. A taper structure is also used to overcome the modes mismatch between the slow light waveguide and “normal”  $W_1$  waveguide. The microwave filter can be used in 60 GHz RoF system to eliminate useless side band.

## 2. Device Design

The configuration of our microwave photonic filter (MPF) based on photonic crystal is shown schematically in Fig. 1. The MPF is consisted of three sections: directional coupler, slow light waveguide and the symmetrical U-shaped waveguides which combined coupler and delay-line. All of them can be fabricated on the same SOI slab with triangular air holes etched. By adjusting the length of directional coupler, the input light is divided into two parts: some light will export along the directional coupler through Light Out port, while the other will transmit into the delay-line PC waveguide through U-shaped bend, and then get back to coupler through the symmetrical U-shaped bends. Since the slow light effect of PC waveguide, the length of MPF can be reduced significantly. For enhancing the coupling strength and decrease the coupler size, smaller holes are introducing in the middle of two waveguides. By perturbing radii and positions of the air holes at the bend corners, we reduce the transmission loss of TE light. We also use PC tapers to decrease the mode mismatch

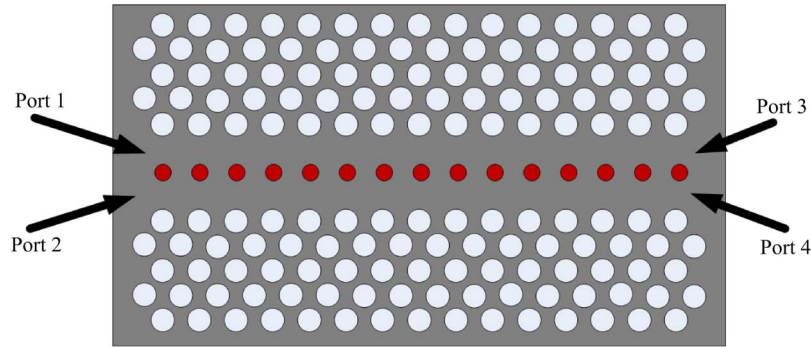


Fig. 2. Schematic view of coupler.

between the normal  $W_1$  waveguide and slow light waveguide, thus the transmission properties of band-edge wavelength can be increased significantly. The incident light is TE polarized, meaning that the optical field has a dominant electric field component  $E_z$  oriented parallel to the substrate plane and perpendicular to the waveguide direction.

### 3. Theory of MPF

A MPF as recirculating loop resonator filter consists of two major parts: directional coupler and delay-line. The schematic of the coupler is shown in Fig. 2. Air holes between the two  $W_1$  waveguides have smaller radii  $rr = 0.30 a$  ( $a$  is the lattice constant), which can decrease the need of coupling length [22]. The mechanism of coupler can be simply explained as coupled mode theory [23]: when transfer through one waveguide, the supermodes coupler lead to incident light power shifting to another waveguide gradually after a beat length [24]. So we can get any coupling efficiency by specifying the length of coupler. If the directional coupler has an appropriate coupling strength, appropriate amount of light would couple to Port 4. After the slow light effect of delay-line, the light get back to the coupler through Port 2, then start the next coupling circulation. Theoretically speaking, the coupling will continue to circulate infinitely. Every circulating provides a basic delay time  $T$  decided by the length and group index of slow light waveguide. The directional coupler has a transmission loss  $\gamma$  given by [25]

$$|E_3|^2 + |E_4|^2 = (1 - \gamma)(|E_1|^2 + |E_2|^2) \quad (1)$$

where  $E_i$  is the complex field amplitude at  $i$  port in Fig. 2,  $\gamma$  is the transmission loss. The complex amplitudes in the waveguides after the coupling are related to the incident-field amplitudes calculated as

$$\begin{aligned} E_3 &= \sqrt{1 - \gamma}(\sqrt{1 - \kappa}E_1 + j\sqrt{\kappa}E_2) \\ E_4 &= \sqrt{1 - \gamma}(\sqrt{1 - \kappa}E_2 + j\sqrt{\kappa}E_1) \end{aligned} \quad (2)$$

where  $\kappa$  is intensity coupling coefficient, it means the percentage composition of the intensity coupling from one waveguide to another. The relationship between  $E_2$  and  $E_4$  can be further explained as:

$$E_2 = E_4\sqrt{1 - \delta}e^{j\beta L}, \quad \beta = 2\pi n_g f/c \quad (3)$$

where  $\delta$  is the delay-line's attenuation coefficient,  $L$  is the length of delay-line slow light PC waveguide,  $n_g$  is the group refractive index,  $f$  is the frequency of incident light, and  $c$  is the light speed in vacuum.

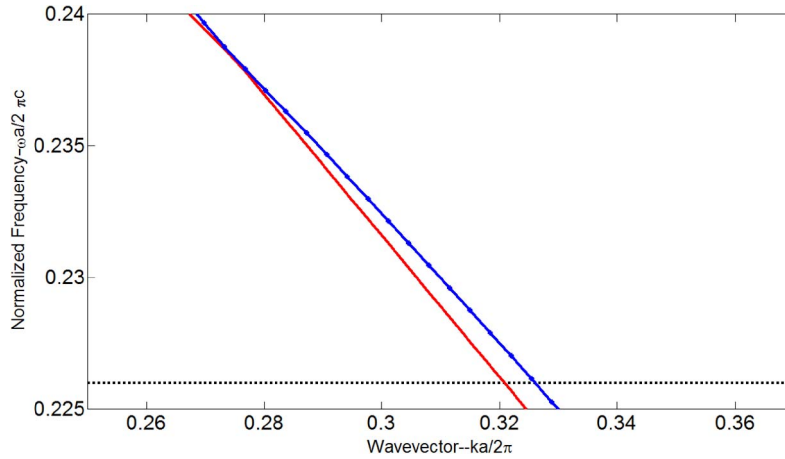


Fig. 3. Photonic band structure of the PC coupler for TE light. Gray dotted line indicates the position of the slow light frequency.

With the values of coupling and delay-line, the simultaneous Eq. (2) and Eq. (3) can be solved to indicate the relationship between Port 3 and Port 1:

$$\frac{E_3}{E_1} = \sqrt{1-\gamma} \left[ \sqrt{1-\kappa} - \frac{\kappa\sqrt{1-\delta}}{e^{-j\beta L} - \sqrt{1-\delta}(1-\gamma)(1-\kappa)} \right]. \quad (4)$$

Depending on above analysis, we can get the transmission of introduced TE light. According to Eq. (4), a series notch peaks appear in the frequency domain. The distance of two adjacent notch peaks can be explained as free spectral range  $FSR = c/n_g L$ . The notch depth based on the values of  $k$  and  $r$  [26]. The analysis provides us an important way to optimize the MPF structure for high performance.

#### 4. Device Optimization

In this section, we will analyze the different parts of the MPF. They are all integrated in the same SOI slab, the effective index of Si is 3.4, the triangular lattice is  $a = 350$  nm, and the radii of common air holes are  $r = 0.35 a$ . The concrete optimizations as shown as follows:

##### 4.1. Optimization of the Coupler and Slow Light Waveguide

Figs. 3 and 4 show the photonic band structure and transmission spectrum of coupler for TE light. The even and odd modes are coupling during transmission, which makes the incident light shift from one waveguide to another. As Fig. 4 shown, the transmission of Port 3 and Port 4 respectively are 0.564 and 0.346. Then we can get the value of intensity coupling coefficient  $\kappa = 0.346/(0.564 + 0.346) = 0.380$ .

Through the above analysis Eq. (2) and Eq. (3), we can see that the group refractive index can influence the length of the delay-line PC when delay time is fixed, which means slow light can greatly enhance the delay effect in the PC structure. On the other hand, when length  $L$  is settled, the relationship between  $n_g$  and FSR is inversely proportional, so we can tune the FSR of filter by change  $n_g$ .

The PC slow light waveguide with circular air holes is shown specifically in Fig. 5. The radius of the first rows of air holes symmetrical adjacent to the waveguide is  $r_1$ , the radius of second rows is  $r_2$  and the common air hole radius is  $r$ . The first rows both vertically and horizontally shift to line defect, while the shifted distances of the air holes are denoted by  $\Delta X$  and  $\Delta Y$ . We denote  $a_1$  as the lattice constant,  $r = 0.32 a_1$ , the background material is silicon.  $D$  is the width of conventional PCW, and the radii of the first two rows of air holes adjacent to the defect are  $r_1$  and  $r_2$ , respectively. The first

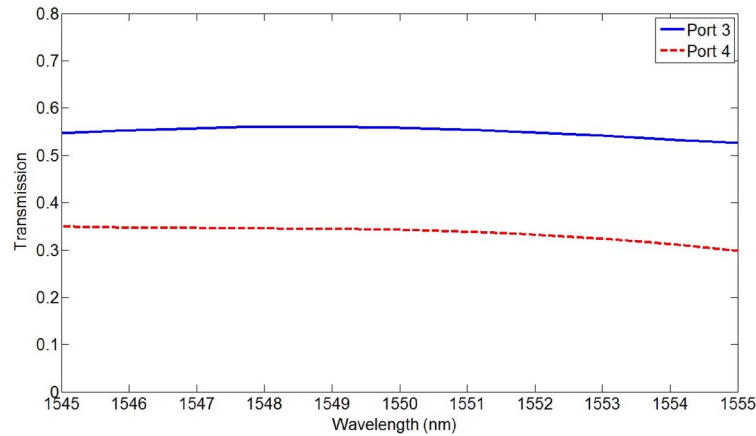


Fig. 4. Transmission spectrum of the proposed coupler PC waveguides.

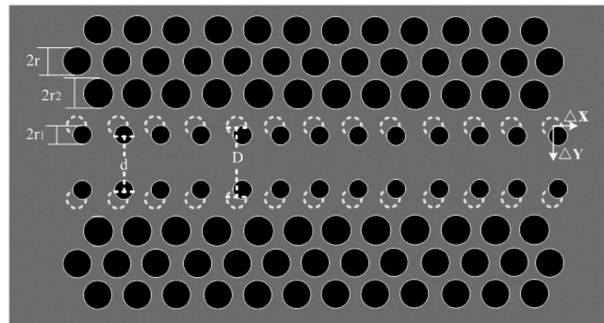


Fig. 5. Schematic view of PC slow light waveguide.

rows are both vertically and horizontally shifted, and the shifted distances of the air holes are denoted by  $\Delta X$  and  $\Delta Y$ .

In order to achieve available slow light properties, we have designed four structures and calculate their parameters. Fig. 6 and Table 1 show the slow light parameters of delay-line PC waveguides, we consider the group index as constant within 10% range, corresponding to Ref. [22]. As the radii  $r_1$  and  $r_2$  increased, the group index curve shifts to higher frequency and higher index. The shift of the first rows can also improve the slow light properties.

From these analyses we can confirm that the slow light properties increase while the wavelengths range decrease. Increasing the negligible dispersion bandwidth will always come at the price of decreased group index and vice versa. Therefore in practical application, when the delay length is fixed, we should design the PC waveguide according to the demand of the FSR and bandwidth for optical wavelength. In the 60G RoF system, we want to use the MPF as a notch filter to eliminate useless side band. So we confirm  $\text{FSR} = 130$  GHz, a little larger than the bandwidth of Double Side Band (DSB). And as the bandwidth need of RoF system is not demanding, we choose structure D to decrease the size of device. According to  $\text{FSR} = c/n_g L$ , the length of slow light waveguide is about  $20.8 \mu\text{m}$ .

#### 4.2. Optimizations of U-Shaped Bend

As we know about the coupler and delay-line, it is necessary to achieve a combined bend with high transmission range covering at least from 1548 nm to 1552 nm. In order to make the two sections integrated well, we demonstrate the bend as Fig. 7 shown. We alter the band structure by

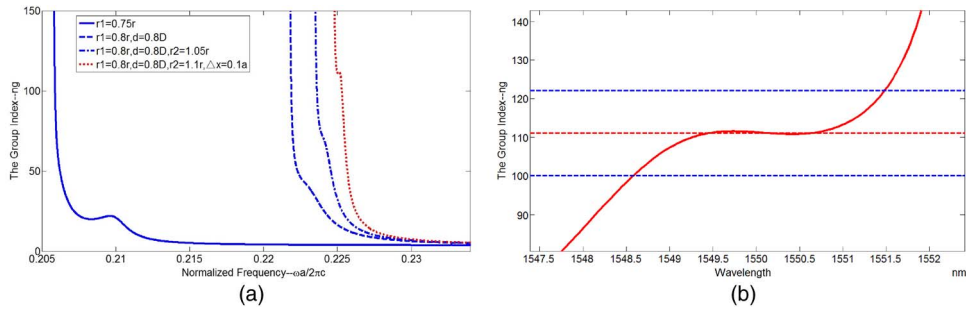


Fig. 6. (a) Group index in terms of normalized frequency with different variables. (b) Enlarged view of group index in terms of wavelength for structure D, where the domain between two blue dotted lines is considered as the flat zone for group index.

TABLE 1

Slow light propertied for different structures

#	$r1$	$r2$	$\Delta y$	$\Delta x$	$n_g$	$\Delta\lambda(nm)$
A	0.283a	0.331a	0	0	20	19
B	0.305a	0.363a	0	0	52	8
C	0.315a	0.375a	0	0	62	7
D	0.321a	0.380a	0.1a	0.05a	111	3

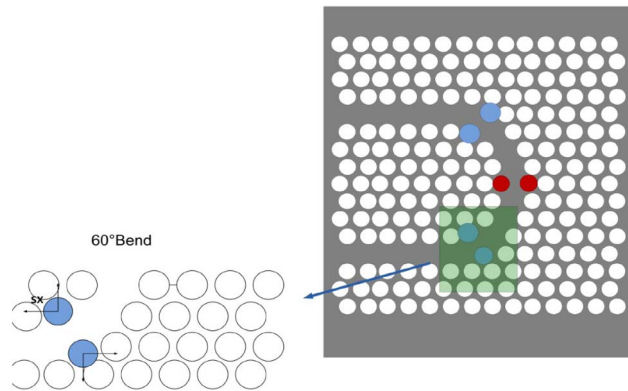


Fig. 7. Schematic view of PC U-shaped bend.

adjusting the radii and positions of air holes near the bend corner. We increase the size of air hole at the inner  $60^\circ$  corner, as  $r_a = 0.36 a$ , and add an air hole at the outer  $60^\circ$  corner, the radius is also  $0.36 a$ . Then we shift  $s_x = 0.15a$  oppositely along the symmetric axis of waveguide. We also change the red air holes in Fig. 7. The radii of red air holes are  $r_b = 0.38 a$ , and they all moved  $0.1 a$  towards the opposite direction of bend.

Since we adjust the structure of U-shaped bend, the mode pattern is similar between bend and straight waveguide. So the light from straight waveguide mostly couple into the bend then introduce

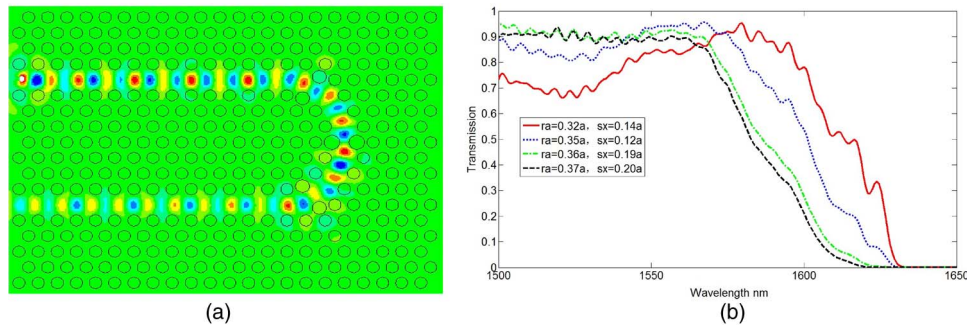


Fig. 8. (a) Steady state electric field profile for the TE-polarized propagating and (b) transmission spectrum of different structure.

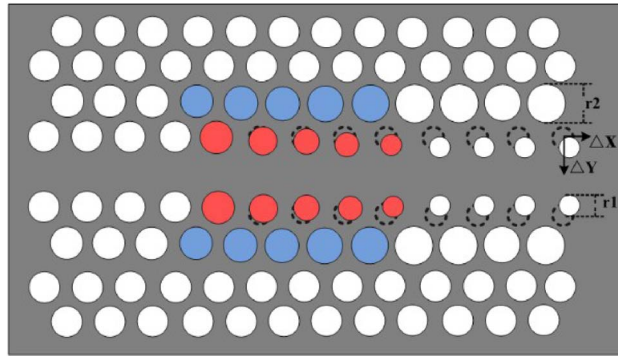


Fig. 9. Schematic of coupled system with taper structure.

into another straight waveguide. The TE light calculated y-component of coupler electric-field ( $E_y$ ) distributions in the x-y plane is shown in Fig. 8(a). In addition, the transmission spectrum calculated by FDTD method is shown in Fig. 8(b). The transmission of the U-shaped bend is 89% for 1550 nm TE light.

#### 4.3. Optimization of the Taper Structure

Optimized PC waveguides can offer a range of frequencies in which guided mode has low group velocity. But the coupling between slow light waveguide and W1 waveguide are still a challenge since the guided modes' mismatch [27]. To solve this problem, we propose a novel PC taper [28], [29], which can significantly increase the transmission properties. As shown in Fig. 9, the PC taper changes gradually from entry to exit, thus are providing no obvious guided mode difference between PC slow light and W1 waveguide. According to the above analyses, the slow light PC waveguide is achieved by adjusting four properties of W1 waveguide: increasing second rods radii to  $r_2$ , decreasing first rods radii to  $r_1$ , and shifting the first rods air holes  $\Delta x$  and  $\Delta y$  along X and Y directions. So our taper structure changes gradually and equably with these four characteristics.

We define the length of taper as  $n - 1$  air holes, thus the characteristics difference between adjacent air holes is  $1/n$  of the total difference between slow light waveguide and W1 waveguide. The coupling performance of different length taper is also calculated, the results are shown in Fig. 10. When  $n$  is less than 6, the coupling performance improves along with the length growth, and almost no obvious change between  $n = 5$  and  $n = 6$ . So we set  $n = 5$ , thus transmission level over 60% is reached up to the band edge, where the transmission for no taper structure coupling system is less than 10%. As shown in Fig. 11, the taper structure can significantly improve the coupling performance.

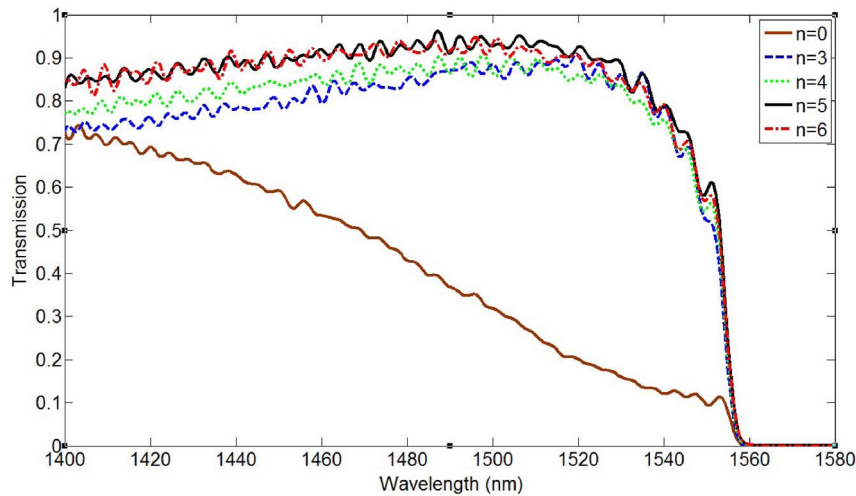


Fig. 10. Transmission spectrum for different length taper structure.

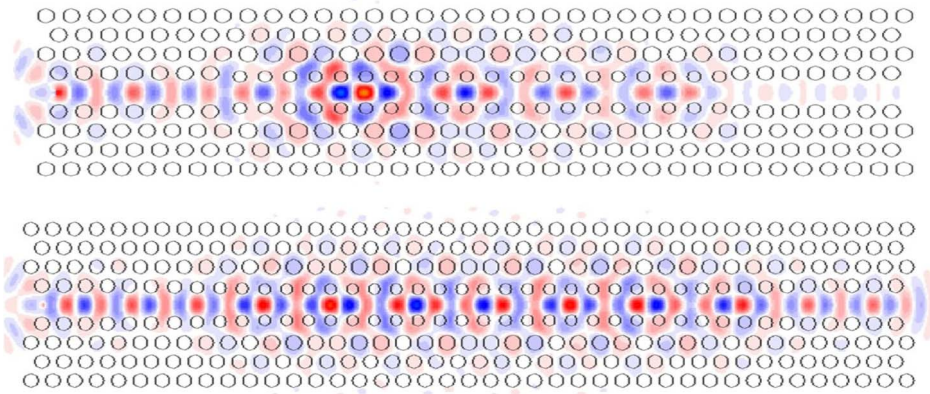


Fig. 11. Steady state electric field profile for the TE-polarized propagating through coupling system. (a) Coupling system with no taper structure, (b) coupling structure with  $n = 5$  taper structure. Input light is 1550 nm TE polarized Gaussian beam.

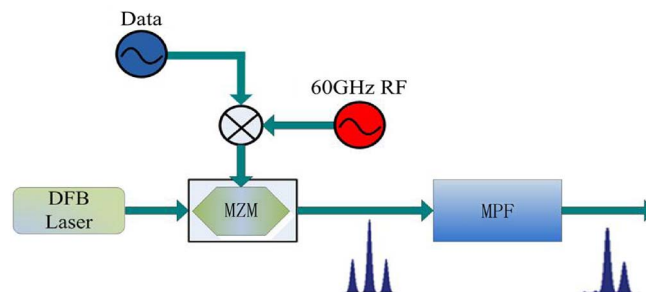


Fig. 12. Block diagram of 60 GHz RoF millimeter wave generator system with MPF.

## 5. Analysis of the MPF Performance

The block diagram of 60GHz RoF millimeter wave generator system is shown in Fig. 12. We use the MPF to separate the carrier and side tones, thus DSB signals become SSB signals. According to the radio frequency and PC slow light waveguide properties, we need a  $20.8 \mu\text{m}$  (60 a) long slow

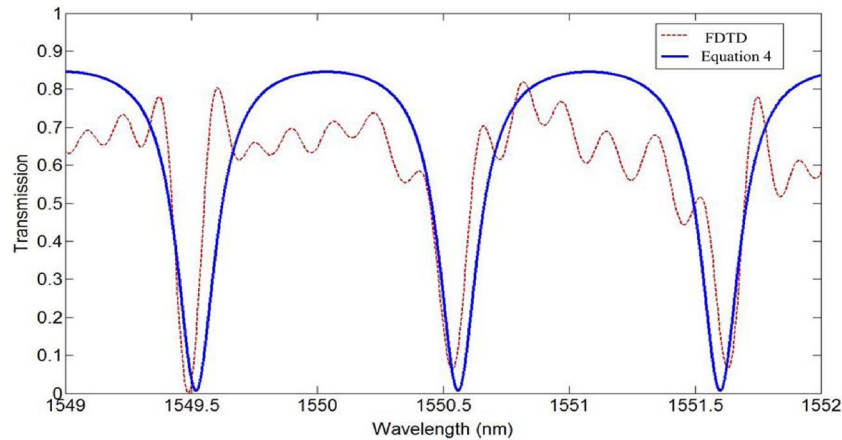


Fig. 13. Transmission spectrum of MPF. The blue line is transmission spectrum calculated by Equation (4) and red dotted curve is calculated by numerical simulations.

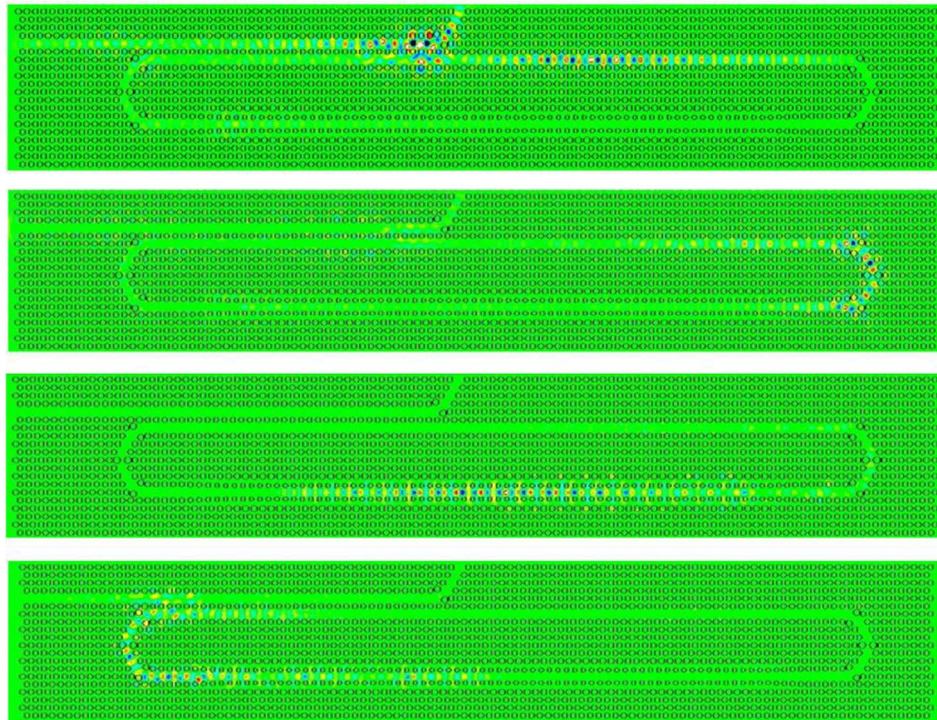


Fig. 14. Steady state electric field profile for the TE-polarized propagating of the MPF at different time ( $t = 84.25 T_0$ ,  $t = 110.75 T_0$ ,  $t = 264.50 T_0$ , and  $t = 450.25 T_0$ ,  $T_0$  is the normalized time unit).

light waveguide. Because of the U-shaped bends and taper structure can also cause time delay (although it is much smaller than the slow light waveguide delay since the different group index), we properly reduce the slow light waveguide length to 54 a through many simulation experiments.

The calculated spectrum results are shown in Fig. 13. It is the transmission performance from input port to output port. The blue line is calculate based on Eq. (4), the variables are set up by above analysis; the red dotted line is calculated by numerical simulations for the total structure. The difference between two transmission curves is caused by the delay time when waves get through the

common waveguide. From the Fig. 13, we can find these two results match well. A pulse traversing the MPF is presented in Fig. 14. The pulse can clearly be seen to circulate through the slow light waveguide.

## 6. Conclusion

In this paper we have proposed a novel photonic crystal based ultra-compact microwave photonic notch filter, which are demonstrated through the PC structure design and simulations. The filter consists of a power coupler, a slow light waveguide and the U-shaped bends connected the each other. With the research of coupled mode theory, we can get coupler properties of coupling coefficient 0.38 and transmission loss 9%. A change in the radii and positions of the air holes adjacent to the waveguide results in a good slow light property of group index  $n_g = 111$ . The optimizations of U-shaped bend and taper structure for slow light waveguide can significantly increase the transmission of 1550 nm TE light in our MPF. From the simulation results, we have demonstrated that the FSR of this MPF is 130 GHz for 60 GHz RoF system and the total length of the device is less than 25  $\mu\text{m}$ , which is much smaller than MPF based on fiber. The quality factor is about 10,000. Besides, the size of these PC based MPF can be decreased by further optimizing the slow light property of PC waveguide, which is an potential advantage of the future optical integrated circuit (OIC) and long-reach radio over fiber system.

---

## References

- [1] Y. Ji, D. Ren, H. Li, X. Liu, and Z. Zheng, "Analysis and experimentation of key technologies in service-oriented optical internet," *Sci. China Inf. Sci.*, vol. 54, no. 2, pp. 215–226, Feb. 2011.
- [2] H.-C. Ji, H. Kim, and Y. C. Chung, "Full-duplex radio-over-fiber system using phase-modulated downlink and intensity-modulated uplink," *IEEE Photon. Technol. Lett.*, vol. 21, no. 1, pp. 9–11, Jan. 2009.
- [3] J. C. Lin, J. Chen, P. Peng, C. Peng, W. Peng, B. Chiou, and S. Chi, "Hybrid optical access network integrating fiber-to-the-home and radio-over-fiber systems," *IEEE Photon. Technol. Lett.*, vol. 19, no. 8, pp. 610–612, Apr. 2007.
- [4] C. W. Chow, C. H. Yeh, M. G. Stanley, C. Li, and H. K. Tsang, "Long-reach radio-over-fiber signal distribution using single-sideband signal generated by a silicon-modulator," *Opt. Exp.*, vol. 19, no. 12, pp. 11 312–11 317, Jun. 2011.
- [5] J. Yu, M. Huang, D. Qian, L. Chen, and G. Chang, "Centralized lightwave WDM-PON employing 16-QAM intensity modulated OFDM downstream and OOK modulated upstream signals," *IEEE Photon. Technol. Lett.*, vol. 20, no. 18, pp. 1545–1547, Sep. 2008.
- [6] N. Deng, C. K. Chan, and L. K. Chen, "A centralized-light-source WDM access network utilizing inverse-RZ downstream signal with upstream data remodulation," *Opt. Fiber Technol.*, vol. 13, no. 1, pp. 18–21, Jan. 2007.
- [7] B. Chmielak, M. Waldow, C. Matheisen, C. Ripperda, J. Bolten, T. Wahlbrink, M. Nage, F. Merget, and H. Kurz, "Fiber dispersion influence on transmission of the optical millimeter-waves generated using LN-MZM intensity modulation," *J. Lightw. Technol.*, vol. 25, no. 11, pp. 3244–3256, Nov. 2007.
- [8] S. Xiao, M. H. Khan, H. Shen, and M. Qi, "A highly compact third-order silicon microring add-drop filter with a very large free spectral range, a flat passband and a low delay dispersion," *Opt. Exp.*, vol. 15, no. 22, pp. 14 765–14 771, Oct. 2007.
- [9] J. Ding, H. Chen, L. Yang, L. Zhang, R. Ji, Y. Tian, W. Zhu, Y. Lu, P. Zhou, R. Min, and M. Yu, "Ultra-low-power carrier-depletion Mach-Zehnder silicon optical modulator," *Opt. Exp.*, vol. 20, no. 7, pp. 7081–7087, Mar. 2012.
- [10] A. Einat and U. Levy, "Analysis of the optical force in the micro ring resonator," *Opt. Exp.*, vol. 19, no. 21, pp. 20 405–20 419, Oct. 2011.
- [11] D. Yang, H. Tian, and Y. Ji, "Nanoscale photonic crystal sensor arrays on monolithic substrates using side-coupled resonant cavity arrays," *Opt. Exp.*, vol. 19, no. 21, pp. 20 023–20 034, Oct. 2011.
- [12] X. Wang, H. Tian, and Y. Ji, "Photonic crystal slow light Mach-Zehnder interferometer modulator for optical interconnects," *J. Opt.*, vol. 12, no. 6, p. 065501, Jun. 2010.
- [13] H. Park, S. Kim, S. Kwon, Y. Ju, J. Yang, J. Baek, S. Kim, and Y. Lee, "Electrically Driven Single-Cell Photonic Crystal Laser," *Science*, vol. 305, no. 5689, pp. 1444–1447, Sep. 2004.
- [14] G. Shen, H. Tian, and Y. Ji, "Ultra-compact ring resonator microwave photonic filters based on photonic crystal waveguides," *Appl. Opt.*, vol. 52, no. 6, pp. 1218–1225, Feb. 2013.
- [15] W. Zheng, M. Xing, G. Ren, and S. G. Johnson, "Integration of a photonic crystal polarization beam splitter and waveguide bend," *Opt. Exp.*, vol. 17, no. 10, pp. 8657–8668, May 2009.
- [16] S. Olivier, H. Benisty, M. Rattier, C. Weisbuch, M. Qiu, A. Karlsson, C. J. M. Smith, R. Houdré, and U. Oesterle, "Resonant and nonresonant transmission through waveguide bends in a planar photonic crystal," *Appl. Phys. Lett.*, vol. 79, no. 16, pp. 2514–2516, Oct. 2001.
- [17] S. Matsuo, A. Shinya, C. Chen, K. Nozaki, T. Sato, Y. Kawaguchi, H. Taniyama, and M. Notomi, "20-Gbit/s directly modulated photonic crystal nanocavity laser with ultra-low power consumption," *Opt. Exp.*, vol. 19, no. 3, pp. 2242–2250, Jan. 2011.
- [18] Y. Guo, L. Yan, W. Pan, B. Luo, and K. Wen, "A plasmonic splitter based on slot cavity," *Opt. Exp.*, vol. 19, no. 15, pp. 13 831–13 838, Jul. 2011.

- [19] R. Hao, E. Cassan, X. Roux, D. Gao, V. Khanh, L. Vivien, and X. Zhang, "Improvement of delay-bandwidth product in photonic crystal slow-light waveguides," *Opt. Exp.*, vol. 18, no. 16, pp. 16 309–16 319, Aug. 2010.
- [20] A. Hosseini, X. Xu, D. Kwong, H. Subbaraman, W. Jiang, and R. Chen, "On the role of evanescent modes and group index tapering in slow light photonic crystal waveguide coupling efficiency," *Appl. Phys. Lett.*, vol. 98, no. 3, pp. 031107-1–031107-3, Jan. 2011.
- [21] C. Bao, J. Hou, H. Wu, C. Eric, L. Chen, D. Gao, and X. Zhang, "Flat band slow light with high coupling efficiency in one-dimensional grating waveguides," *Photon. Technol. Lett.*, vol. 24, no. 1, pp. 7–9, Jan. 2012.
- [22] T. Liu, A. R. Zakharian, M. Fallahi, J. V. Moloney, and M. Mansuripur, "Design of a compact photonic-crystal-based polarizing beam splitter," *IEEE Photon. Technol. Lett.*, vol. 17, no. 7, pp. 1435–1437, Jul. 2005.
- [23] S. Boscolo, M. Midrio, and C. G. Someda, "Coupling and decoupling of electromagnetic waves in parallel 2-D photonic crystal waveguides," *IEEE J. Quantum Electron.*, vol. 38, no. 1, pp. 47–53, Jan. 2002.
- [24] S. G. Johnson, P. Bienstman, M. A. Skorobogatiy, M. Ibanescu, E. Lidorikis, and J. D. Joannopoulos, "Adiabatic theorem and continuous coupled-mode theory for efficient taper transitions in photonic crystals," *Phys. Rev. E*, vol. 66, no. 6, p. 066608, Dec. 2002.
- [25] L. F. Stokes, M. Chodorow, and H. J. Shaw, "All-single-mode fiber resonator," *Opt. Lett.*, vol. 7, no. 6, pp. 288–290, Jun. 1982.
- [26] F. Long, H. Tian, and Y. Ji, "A study of dynamic modulation and buffer capability in low dispersion photonic crystal waveguides," *J. Lightw. Technol.*, vol. 28, no. 8, pp. 1139–1143, Apr. 2010.
- [27] P. Pottier, I. Ntakis, and R. M. Rue, "Photonic crystal continuous taper for low-loss direct coupling into 2D photonic crystal channel waveguides and further device functionality," *Opt. Commu.*, vol. 223, no. 4–6, pp. 339–347, Aug. 2003.
- [28] P. Bienstman, S. Assefa, S. G. Johnson, J. D. Joannopoulos, G. S. Petrich, and L. A. Kolodziejski, "Taper structures for coupling into photonic crystal slab waveguides," *J. Opt. Soc. Amer. B*, vol. 20, no. 9, pp. 1817–1821, Sep. 2003.
- [29] P. Pottier, M. Gnan, and R. M. Rue, "Efficient coupling into slow-light photonic crystal channel guides using photonic crystal tapers," *Opt. Exp.*, vol. 15, no. 11, pp. 6569–6575, May 2007.